Draft version August 21, 2020
Typeset using LaTeX default style in AASTeX63

On the Scaling Properties of Magnetic Field Fluctuations Through the Inner Heliosphere

Tommaso Alberti,[1] Monica Laurenza,[1] Giuseppe Consolini,[1] Anna Milillo,[1] Maria Federica Marcucci,[1] Vincenzo Carbone,[2] and Stuart D. Bale[3,4]

[1] *INAF - Istituto di Astrofisica e Planetologia Spaziali, via del Fosso del Cavaliere 100, 00133, Roma, Italy*
[2] *Università della Calabria, Dip. di Fisica, Ponte P. Bucci, Cubo 31C, 87036, Rende (CS), Italy*
[3] *Space Sciences Laboratory, University of California, Berkeley, CA 94720-7450, USA*
[4] *Physics Department, University of California, Berkeley, CA 94720-7300, USA*

(Received; Revised; Accepted)

Submitted to ApJ

ABSTRACT

Although the interplanetary magnetic field variability has been extensively investigated *in situ* by means of data coming from several space missions, the newly launched missions providing high-resolution measures and approaching the Sun, offer the possibility to study the multiscale variability in the innermost solar system. Here by means of the Parker Solar Probe measurements we investigate the scaling properties of solar wind magnetic field fluctuations at different heliocentric distances. The results show a clear transition at distances close to say 0.4 au. Closer to the Sun fluctuations show a $f^{-3/2}$ frequency power spectra and regular scaling properties, while for distances larger than 0.4 au fluctuations show a Kolmogorov spectrum $f^{-5/3}$ and are characterized by anomalous scalings. The observed statistical properties of turbulence suggests that the solar wind magnetic fluctuations, in the late stage far form the Sun, show a multifractal behaviour typical of turbulence and described through intermittency, while in the early stage, when leaving the solar corona, a breakdown of these properties are observed, thus showing a statistical monofractal global self-similarity. Physically the breakdown observed close to the Sun should be due either to a turbulence with regular statistics or to the presence of intense stochastic fluctuations able to cancel out correlations necessary for the presence of anomalous scaling.

Keywords: Sun: magnetic fields — Sun: solar wind — methods: data analysis — methods: statistical — turbulence

1. INTRODUCTION

Since the 70s several space missions have been launched to provide new insights into the solar phenomena and solar wind properties (e.g., Helios, Ulysses, Wind, ACE) allowing us to collect a wide amount of data about the processes that cause the solar wind formation and evolution throughout the interplanetary space (e.g., Rosenbauer et al. 1977; Denskat & Neubauer 1982; Grappin et al. 1990). Among other topics (e.g., Burlaga et al. 1982; McComas et al. 1995; Marsch 2018), a wide attention has been paid to turbulence in the solar wind by investigating the scaling behavior of both velocity and magnetic field components (e.g., Dobrowolny et al. 1980; Matthaeus & Goldstein 1982; Tu & Marsch 1990; Bruno & Carbone 2013; Alberti et al. 2019a, and references therein). Indeed, solar wind magnetic field fluctuations around the large-scale mean field, usually described within the magnetohydrodynamic (MHD) framework, are characterized by scale-invariant features over a wide range of scales (e.g., Bruno & Carbone 2013). At 1 au, this range of scales, known as inertial range (Kolmogorov 1941; Frisch 1995), is dominated by Alfvénic fluctuations (Belcher 1971; Bruno & Carbone 2013) mixed with slow mode compressive ones (Howes et al. 2012; Klein et al.

Corresponding author: Tommaso Alberti
tommaso.alberti@inaf.it

2012; Verscharen et al. 2017). This type of turbulence is characterized by an anisotropic cascade (Horbury et al. 2008; Chen 2016), mostly described by models of balance and imbalanced Alfvénic turbulence (Lithwick et al. 2007; Perez & Boldyrev 2009; Chandran et al. 2015; Mallet & Schekochihin 2017), although different scalings are observed depending on several features as the role of the large-scale forcing (Velli et al. 1989), the (im)balance between Alfvénic fluctuations (Boldyrev 2006; Chandran et al. 2015; Mallet & Schekochihin 2017), and so on (Chen 2016; Chen et al. 2020). Moving closer to the Sun, a decreasing scaling slope is observed with a transition mostly occurring near 0.4 au (Dobrowolny et al. 1980; Denskat & Neubauer 1982; Tu & Marsch 1990; Chen et al. 2020), the inertial range tends to move towards a more steady state (Chen et al. 2020), an increase in the scale-dependent alignment and cross-helicity is also observed (Boldyrev 2006; Lithwick et al. 2007), together with a different nature of the nonlinear coupling between different frequencies and/or damping/propagation effects (e.g., Dobrowolny et al. 1980). Moreover, as the Sun is approached an increase of up to two order of magnitude is observed for turbulence energy, together with less steep spectra for magnetic field components, the velocity field and the Elsässer variables, being characterized by a spectral exponent closer to -3/2 (Chen et al. 2020). Furthermore, the role of slow-mode fluctuations tend to be reduced as for the rate of compressible magnetic fluctuations, while outward-propagating Alfvénic perturbations dominate on inward-propagating ones, consistent with turbulence-driven models (Boldyrev 2006; Chandran et al. 2015; Mallet & Schekochihin 2017).

Nowadays, a large amount of spacecraft, providing more accurate in situ measurements through high-resolution instruments, is available for monitoring the evolution of solar wind parameters and for providing new insights into the physics of the Sun and the solar wind. Furthermore, the different locations and orbits of these spacecraft could offer the possibility of investigating some interesting properties of solar wind turbulence and its evolution throughout the heliosphere (e.g., Nicolaou et al. 2019), especially going as near as possible to the solar surface (Marsden & Fleck 2003; Fox et al. 2016). The recently launched missions, e.g., *Parker Solar Probe* (PSP), *BepiColombo*, and *Solar Orbiter*, and the in situ orbiting ones, e.g., ACE, Wind, and STEREO, offer the unique opportunity of multi-spacecraft combined observations of the interplanetary medium variability, the evolution of turbulence and solar wind structures at different distances from the Sun, the interaction between the solar wind plasma and planetary environments, and so on (e.g., Milillo et al. 2010; Müller et al. 2013; Howard et al. 2019; Kasper et al. 2019; McComas et al. 2019). Recently, in the framework of solar wind turbulence Chen et al. (2020) investigated the behavior of the power spectral density at different heliocentric distances by means of the first two orbits of the Parker Solar Probe spacecraft showing that the power-law spectral index moves from $\alpha_B \sim$ -3/2 to $\alpha_B \sim$ -5/3 when passing from $r \sim 0.17$ au to $r \sim 0.6$ au.

In this manuscript we deal with the analysis of the interplanetary magnetic field fluctuations along the PSP trajectory during its first and second orbits towards the Sun by means of a novel formalism based on the Hilbert Spectral Analysis (HSA). Specifically, we investigate the $q-$order scaling features of magnetic field components at different heliocentric distances (Section 3). In Section 4, the results show that the inertial range scaling properties significantly change when moving from closer to farther the Sun, with intermittency completely emerging at distances larger than 0.4 au. Indeed, scaling exponents show a linear behavior at smaller heliocentric distances, while larger exponents characterized by a nonlinear convex behavior with the statistical order q are found at $r > 0.4$ au. In Section 5, we conclude that the result of this study could open new perspectives for describing the fractal properties of solar wind and to correctly characterize turbulence and intermittency in space plasmas at different locations.

2. DATA

For this study we use solar wind magnetic field components in the heliocentric RTN reference frame (R=radial, T=tangential, N=normal) as measured by the PSP magnetometer. The PSP magnetic field data are taken by the outboard FIELDS Fluxgate Magnetometer (MAG) (Bale et al. 2016, 2019) and are averaged to 1-s cadence from their native 4 samples per cycle cadence (Fox et al. 2016). Data were freely retrieved from the Space Physics Data Facility (SPDF) Coordinated Data Analysis Web (CDAWeb) interface at https://cdaweb.gsfc.nasa.gov/index.html/.

For investigating the evolution of the interplanetary magnetic field we used the first and the second orbit of PSP towards the Sun, only considering adjacent temporal measurements during which no data gaps were found (i.e., the best time coverage of the FIELDS instrument). These corresponds to the period between 15 October and 04 December, 2018, and between 16 March and 10 April, 2019, for the first and the second orbits, respectively. During the intervals of investigation the solar wind speed was between 250 km/s and 650 km/s and the proton density ranged between $n \sim 10$ cm^{-3} (at 0.7 au) and ~ 400 cm^{-3} (at 0.17 au). Figure 1 shows the three components of the interplanetary magnetic field (at 1-s resolution) and the PSP radial distance from the Sun (at 1-hr resolution).

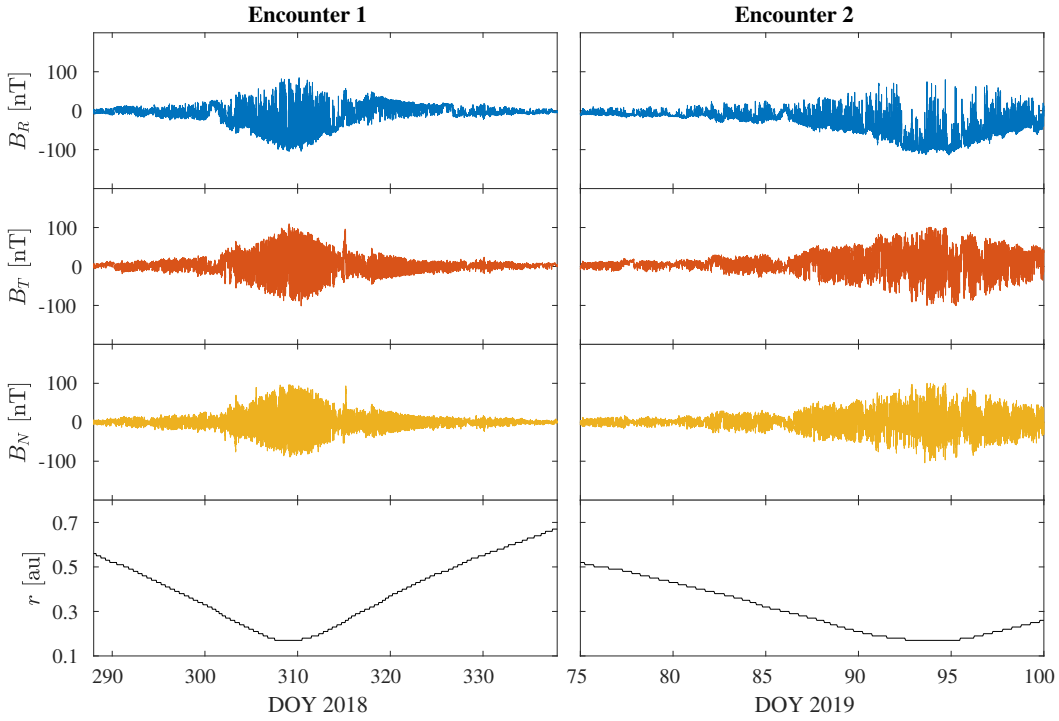

Figure 1. (From top to bottom) The three components of the interplanetary magnetic field (at 1-s resolution), and (lower panel) the PSP radial distance from the Sun (at 1-hr resolution). The blue, orange, and yellow lines refer to the radial, tangential, and normal components, respectively. The right and the left panels show measurements during the first and the second PSP orbits approaching the Sun, respectively.

It is clear that magnetic field fluctuations decrease with increasing heliocentric distance of about one order of magnitude (i.e., $B(r) \sim 1/r^2$, Parker 1958). However, by simply looking at the time series it is not sufficient to clearly discriminate between the different dynamical regimes and their evolution at different heliocentric distances, that is a crucial point for correctly characterizing dynamical processes such as the evolution of turbulence and intermittency, the large-scale structures dynamics, the mean field approximation, and so on.

3. METHODS

Investigating field fluctuations is usually one of the most important aspects of dealing with the existence of dynamical processes and phenomena characterizing physical systems. Generally, this can be achieved by means of data analysis methods allowing us to extract embedded features from several kinds of data and by assuming some mathematical assumptions (e.g., Huang et al. 1998). Obviously, a suitable and well-built data analysis method should require to minimize mathematical assumptions and numerical artifacts, trying to maximize its adaptivity to the data under investigation (e.g., Huang et al. 1998). A suitable method with the above characteristics is the well-known and well-established Hilbert-Huang Transform (HHT), firstly introduced by Huang et al. (1998) as an adaptive and a posteriori data analysis procedure, mainly based on two different steps: a decomposition method, known as Empirical Mode Decomposition (EMD), and a statistical spectral method, e.g., the HSA (e.g., Huang et al. 1998).

The first step of the HHT, e.g., the EMD, allows us to derive from the original signal $B_\mu(t)$ (being $B_\mu(t)$ the μ-th component of the interplanetary magnetic field) the set of empirical modes $\mathcal{C}_{\mu,k}(t)$. They are defined as functions having the same (or differing at most by one) number of extrema and zero crossings and a zero-average mean envelope and are obtained by means of the so-called sifting process based on the following steps:

1. define the zero-mean signal $B_{\mu_m}(t) = B_\mu(t) - \langle B_\mu(t) \rangle$, being $\langle \ldots \rangle$ the average value;
2. find the local extrema of $B_{\mu_m}(t)$;
3. find the upper $\mathcal{U}(t)$ and the lower $\mathcal{L}(t)$ envelopes by using a cubic spline;
4. find the mean envelope $\rightarrow \mathcal{M}(t) = \frac{\mathcal{U}(t)+\mathcal{L}(t)}{2}$;

5. define $\mathcal{D}_\mu(t) = B_{\mu_m}(t) - \mathcal{M}(t)$;

6. **if $\mathcal{D}_\mu(t)$ is an empirical mode then**

   6.1 store $\mathcal{C}_{\mu,k}(t) = \mathcal{D}_\mu(t)$;

   6.2 $B_{\mu_m}(t) \rightarrow B_{\mu_m}(t) = B_{\mu_m}(t) - \mathcal{D}_\mu(t)$;

   6.3 repeat steps 1.-5;

6. **if $\mathcal{D}_\mu(t)$ is not an empirical mode then**

   6.1 iterate steps 1.-5. until $\mathcal{D}_\mu(t)$ is an empirical mode;

   6.2 store $\mathcal{C}_{\mu,k}(t) = \mathcal{D}_\mu(t)$;

   6.3 $B_{\mu_m}(t) \rightarrow B_{\mu_m}(t) = B_{\mu_m}(t) - \mathcal{D}_\mu(t)$;

   6.4 repeat steps 1.-5;

7. stop the process when $\mathcal{R}_\mu(t) = \mathcal{D}_\mu(t)$ is a non-oscillating function or has only two extrema.

Thus, a completely adaptive procedure is built, there are no assumptions and requirements on linearity and/or stationarity of $B_\mu(t)$, and the decomposition basis $\{\mathcal{C}_{\mu,k}(t)\}$ is a complete and orthogonal set, as for usual decomposition methods (e.g., Fourier analysis or Wavelets, Huang et al. 1998). This means that we can write

$$B_\mu(t) = \sum_{k=1}^{N} \mathcal{C}_{\mu,k}(t) + \mathcal{R}_\mu(t), \tag{1}$$

being $\mathcal{C}_{\mu,k}(t)$ the k-th empirical mode, and $\mathcal{R}_\mu(t)$ the residue of the decomposition, e.g., a non-oscillating function (e.g., Huang et al. 1998).

The second step of the HHT is to investigate the amplitude and frequency modulation of each empirical mode by means of the so-called Hilbert Transform (HT) which is defined as

$$\hat{\mathcal{C}}_{\mu,k}(t) = \frac{1}{\pi}\mathcal{P}\int_0^\infty \frac{\mathcal{C}_{\mu,k}(t')}{t-t'}dt', \tag{2}$$

where $\mathcal{P}$ is the Cauchy principal value (e.g., Huang et al. 1998). Then, by defining

$$\mathcal{Z}_{\mu,k}(t) = \mathcal{C}_{\mu,k}(t) + i\,\hat{\mathcal{C}}_{\mu,k}(t) = \mathcal{A}_{\mu,k}(t)e^{i\,\Phi_{\mu,k}(t)}, \tag{3}$$

we can derive

$$\mathcal{C}_{\mu,k}(t) = \Re\left\{\mathcal{Z}_{\mu,k}\right\} = \mathcal{A}_{\mu,k}(t)\cos\left[\Phi_{\mu,k}(t)\right], \tag{4}$$

$$\mathcal{A}_{\mu,k}(t) = \sqrt{\mathcal{C}^2_{\mu,k}(t) + \hat{\mathcal{C}}^2_{\mu,k}(t)}, \tag{5}$$

$$\Phi_{\mu,k}(t) = \tan^{-1}\left[\frac{\hat{\mathcal{C}}_{\mu,k}(t)}{\mathcal{C}_{\mu,k}(t)}\right], \tag{6}$$

being $\mathcal{A}_{\mu,k}(t)$ and $\Phi_{\mu,k}(t)$ the instantaneous amplitude and phase of the $k-$th empirical mode, respectively, thus $\mathcal{C}_{\mu,k}(t)$ is modulated both in amplitude and phase (e.g., Huang et al. 1998). Moreover, we can simply define the instantaneous frequency as $f_{\mu,k}(t) = \frac{1}{2\pi}\frac{d\Phi_{\mu,k}(t)}{dt}$ and the mean timescale $\tau_{\mu,k} = \langle f^{-1}_{\mu,k}(t)\rangle_t$, with $\langle\ldots\rangle_t$ identifying the time average.

Despite the above interesting properties and features of the HHT, surely helpful for correctly identifying the multiscale behavior of physical systems (e.g., Alberti et al. 2018; Laurenza et al. 2019; Alberti et al. 2020), the HHT is particularly helpful for investigating spectral and scaling features from a statistical point of view (e.g., Huang et al. 2011). Indeed, the combination of both EMD and HSA allows us to investigate how the energy content of a signal $B_\mu(t)$ evolves over different frequencies (i.e., at different timescales, allowing us a multiscale characterization) and at different times (e.g., Huang et al. 1998). This can be simply achieved by contouring in a time-frequency plane the square of instantaneous amplitudes of each empirical mode, thus defining the so-called Hilbert-Huang spectrum (Huang et al. 1998)

$$\mathcal{H}(t,f) = \mathcal{A}^2(t,f). \tag{7}$$

The latter has a completely different meaning of energy spectra defined by means of other decomposition techniques, (e.g., Fourier or Wavelet spectrograms, Huang et al. 1998). Indeed, while for fixed scale decomposition methods the existence of energy at a frequency means that a component at that scale persisted through the whole time range, for the HHT it means that, in the whole time range, there is a higher likelihood for such a wave to have appeared locally, since frequency varies with time (e.g., Huang et al. 1998). This is a direct consequence of the new concept of instantaneous frequency, thus implying that finding a frequency value $f^\star$ simply means that within the whole set of values of $f_{\mu,k}(t)$, $k = 1, \ldots, N$, there is a higher likelihood of finding the value $f^\star$ at the time $t^\star$ with a probability of $\mathcal{H}(t^\star, f^\star)$ (e.g., Huang et al. 1998). Thus, the Hilbert-Huang spectrum acquires a statistical meaning, instead of having a more deterministic sense as for previous methods (e.g., Huang et al. 1998).

The concept can be rapidly expanded to all statistical moments of the instantaneous amplitudes probability distribution functions such that we can define (e.g., Huang et al. 2011), for a given moment order $q \geq 0$,

$$\mathcal{H}_q(t, f) = \mathcal{A}^q(t, f). \tag{8}$$

As usual in statistics, by keeping fixed $q = 2$ we account for the distribution of energy (e.g., the variance) at different frequencies f and for any time t, and by integrating over time we account for the global energy distribution at different frequencies

$$\mathcal{H}_2(f) = \int_0^T \mathcal{H}_2(t', f) dt', \tag{9}$$

known as Hilbert marginal spectrum (Huang et al. 1998), directly related to the Fourier spectrum (e.g., Huang et al. 2011). Finally, as firstly shown by Huang et al. (2011) the generalized Hilbert-Huang spectra $H_q(t, f)$ can be powerfully used to investigate scaling law behavior of time series as well as to characterize fractal properties due to their analogy with standard structure function analysis (e.g., Huang et al. 2011; Consolini et al. 2017; Carbone et al. 2018). Indeed, by integrating over time we can define

$$\mathcal{S}_q(f) = \int_0^T \frac{\mathcal{H}_q(t', f)}{f} dt' \tag{10}$$

whose scaling behavior is equivalent to that of the generalized structure functions $S_q(\tau) = |B_\mu(t + \tau) - B_\mu(t)|^q$ (e.g, Huang et al. 2011; Carbone et al. 2018). However, due to its local nature, $\mathcal{S}_q(f)$ allows to determine scaling properties by reducing the effect of the noise, large-scale structures and inhomogeneities, and sampling effects (e.g., Huang et al. 2011). While for structure functions the scaling behavior can be characterized by means of scaling exponents ζ_q as

$$S_q(\tau) \sim \tau^{\zeta_q}, \tag{11}$$

for the HSA we have that

$$\mathcal{S}_q(f) \sim f^{-\beta_q}, \tag{12}$$

being (e.g., Huang et al. 2011)

$$\beta_q = \zeta_q + 1. \tag{13}$$

Furthermore, if the exponents β_q linearly behave with the order q over a frequency range $f \in [f_1, f_2]$ then the process occurring within this range of frequencies is monofractal, while if β_q is a nonlinear convex function of q then it shows multifractal features (e.g., Consolini et al. 2017; Carbone et al. 2018).

As stated above the generalized Hilbert spectra are totally equivalent to the approach proposed by the classical canonical structure function analysis which has been widely used for characterizing solar wind scaling properties (e.g., Carbone 1994; Politano et al. 1998; Bruno & Carbone 2013). However, there are some main drawbacks of structure function (SF) analysis which need to be fixed and/or properly considered when searching for scaling law behaviors. Indeed, the measure of scale-invariant features over a specific range of scales by using the SF analysis is largely influenced by trends. This is due to the fact that, although increments/differences are local in the physical domain, in the frequency one they are still global, while the **HHT** allows to overcome this limitation due to its local nature in the time **(thanks to the EMD)** and in the frequency **(thanks to the HSA)** domains, respectively, due to its completely self-adaptiveness property (Huang et al. 1998, 2011). Moreover, the SF analysis is also particularly sensitive to possible external source mechanisms and forcings operating on larger scales than those considered for evaluating scaling properties. Indeed, it has been proved by Huang et al. (2008, 2009) that strong deterministic forcings had an

important influence on classical methods as SF, wavelet-based methods, or multifractal detrended fluctuation analysis, whereas the HSA is much more stable, thus being more appropriate for time series showing multiscale variability with different complexity properties, including trends, external forcing mechanisms, periodic components, and so on (Huang et al. 2009), thanks to the adaptive and local approach at the heart of the HSA (Huang et al. 1998). The above features and effects could also be observed during the PSP orbits since PSP observed numerous magnetic switchback structures which can have profound impact on scale-invariant features and spectral properties. They are associated with large-amplitude fluctuations closer to the Sun (Chen et al. 2020) and could represent a remnant of driving processes at the Sun could affect the energy cascade as the solar wind expands (Bale et al. 2019), although their origin and role in the turbulent cascade remain an open question. However, while classical methods could be affected by these driving processes, the adaptive and local nature of the HSA allows to deal with these structures by filtering them out and hence leading to a better evaluation of scaling/spectral exponents with respect to the SF analysis (Zhao et al. 2020). Thus, the HSA provides a powerful way to characterize scaling properties in an amplitude-frequency space and also a novel framework for investigating multifractality and intermittency, likely applicable to different fields (Huang et al. 2008, 2009, 2011; Consolini et al. 2017; Carbone et al. 2018, 2019).

4. RESULTS & DISCUSSION

We begin our analysis by looking at the behavior of the dimensionality of the system as the heliocentric distance varies which also allows to investigate how anisotropy evolves with r. To do this, we evaluate the eigenvalues λ_i of the covariance matrix $C_{ij} = \langle B_i B_j \rangle - \langle B_i \rangle \langle B_j \rangle$ at different heliocentric distances by making use of overlapping windows of length 1 day at 1-hr steps. This allows to consider how the anisotropy and the dimensionality of the unstable fixed point of MHD equations, i.e., the inertial range (Bruno & Carbone 2013; Alberti et al. 2019b, 2020), radially evolve by looking at the behavior of the quantity $D = \frac{\sum_{i=1}^{3} \lambda_i}{\lambda_3}$, assuming the eigenvalues in the increasing order $\lambda_i \leq \lambda_j$ if $i \leq j$. Figure 2 reports the behavior of D as a function of the heliocentric distance r.

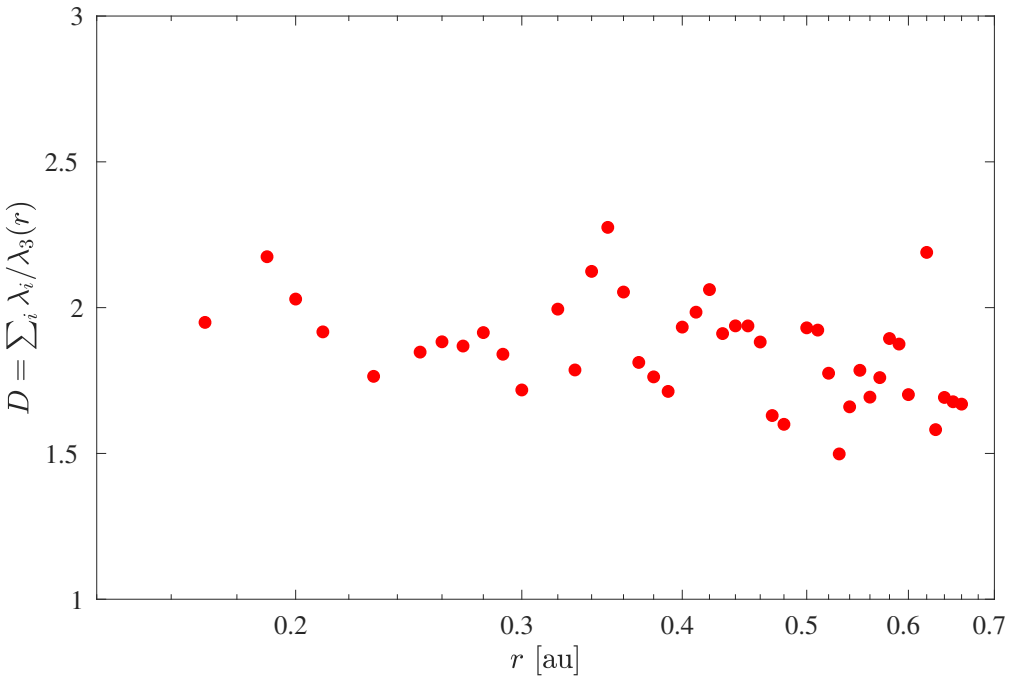

Figure 2. The behavior of the dimensionality $D = \sum_i \lambda_i/\lambda_3(r)$ of the system as a function of the heliocentric distance r.

The results clearly show how **the dimension of the magnetic field fluctuations across the inertial range is essentially 2**, especially as the Sun is approached, that is compatible with a 2D Reduced MHD (RMHD) scenario, also considering the increasing strength of the magnetic field as closer to the Sun (Bruno & Carbone 2013). This **can be related to** the mostly slow nature of solar wind encountered by PSP during the first two orbits (as in the present

study and for larger r) and with a high Alfvénic nature as the Sun is approached (Chen et al. 2020). Moreover, since the ratio between the solar wind speed and the Alfvén speed was larger than 3 (1) for a great (whole) part of the first two orbits our results in the time domain cannot be simply related/interpreted in the spatial domain. Nevertheless, there is a correspondence between the frequency and the wavenumber spectra of the outward-propagating component of highly imbalanced turbulence via the Taylor hypothesis (Klein et al. 2012), or due to the sweeping by larger-scale eddies when the Taylor hypothesis breaks down (Perez & Boldyrev 2009; Chen et al. 2020). In this sense our results can be spatially interpreted and suggest that there is a strong anisotropy in the magnetic field fluctuations across the inertial range.

It has been widely shown that solar wind magnetic field fluctuations are characterized by a scaling law behavior in a wide range of frequencies, supporting the existence of an inertial regime where energy is transferred through an inviscid mechanism to higher frequencies (e.g., to smaller scales, Kolmogorov 1941; Iroshnikov 1965; Kraichnan 1965; Bruno & Carbone 2013). As recently pointed out by Chen et al. (2020) spectral exponents move from $\alpha_B \sim$ -3/2 to $\alpha_B \sim$ -5/3 when passing from $r \sim 0.17$ au to $r \sim 0.6$ au, thus supporting the existence of a different energy transfer across scales for frequencies $f \in [10^{-3}, 10^{-1}]$ Hz compatible with models of inertial range MHD turbulence (Chen et al. 2020). By means of the HHT we are able to investigate the behavior of scaling exponents $\zeta_q = \beta_q - 1$ of magnetic field components, at different heliocentric distances, by evaluating them for overlapping windows, at 1-hr steps, of length 1 day over the inertial range for all data segments. As suggested by Dudok (2004) we perform our q-order analysis up to $q_{max} = 5$ that is the maximum order q to accurately determine q-order statistics estimated via the empirical criterion $q_{max} = \log N - 1 = \log 10^6 - 1 = 5$, with being N the number of data points. Figure 3 show the behavior of $\zeta(2)$ as a function of the heliocentric distance, together with the 95% confidence level.

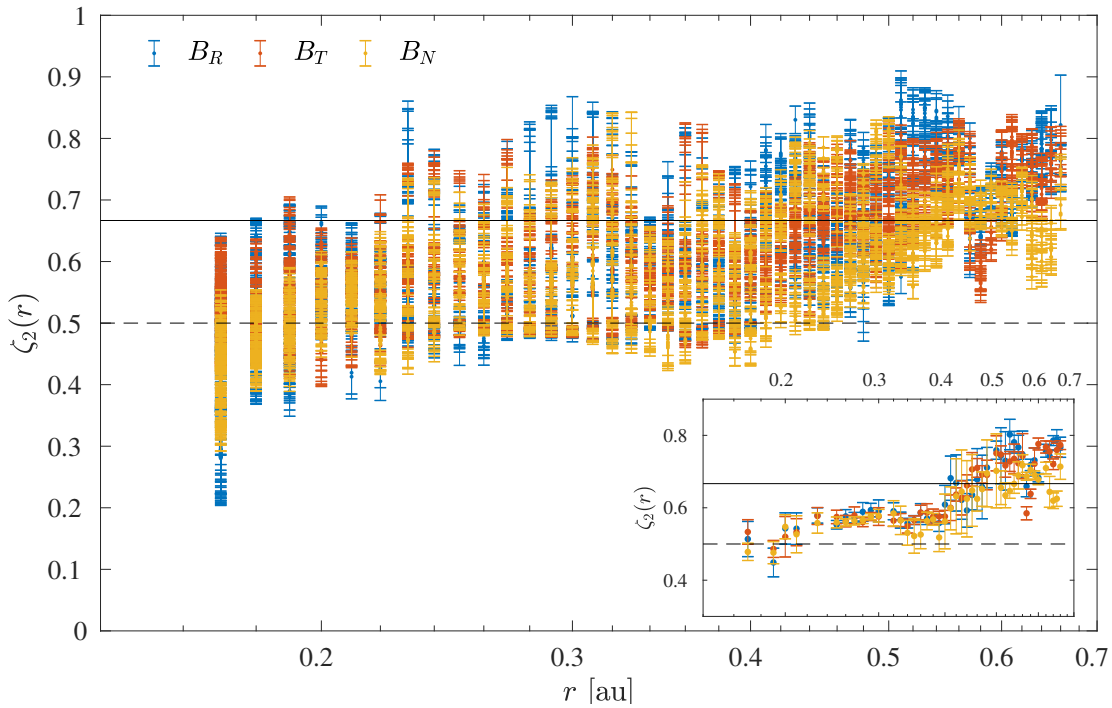

Figure 3. The behavior of the scaling exponents ζ_2 for each magnetic field component at different heliocentric distances r, together with the 95% confidence level. The blue, orange, and yellow symbols refer to the radial B_R, tangential B_T, and normal B_N components, respectively. The continuous and dashed black lines are used as a reference to 2/3 (Kolmogorov 1941) and 1/2 (Iroshnikov 1965; Kraichnan 1965) theoretical values, respectively. The inset show running averages at different heliocentric distances with a step $\Delta r = 0.01$ au (error bars are evaluated as the standard deviations).

Results clearly show a difference between the scaling exponents ζ_2 for distance below 0.4 au with respect to those evaluated at larger distances (i.e., larger than 0.4 au). This difference suggests that magnetic field fluctuations follows a $f^{-3/2}$ scaling closer to the Sun, being $\zeta_2 \simeq 1/2$, while a steeper scaling is found at larger distances ($\zeta_2 \simeq 2/3$ for

$r > 0.4$ au). These findings are consistent with those reported by Denskat & Neubauer (1982) and Tu & Marsch (1990) using Helios data, and more recently by Chen et al. (2020) using PSP data. The lower ζ_2 observed near the Sun could be related to a more steady-state nature of the inertial range, due to the large number of nonlinear times (Matthaeus & Goldstein 1982). Conversely, the larger values of ζ_2 at $r > 0.4$ au can be related to a reduced value of the normalized cross-helicity as r increases as well as to the role of intermittency (Bruno & Carbone 2013). Both findings are also well in agreement with predictions made by numerical simulations of Alfvénic turbulence in homogeneous plasmas (Boldyrev 2006; Lithwick et al. 2007; Perez & Boldyrev 2009; Chandran et al. 2015; Mallet & Schekochihin 2017), suggesting that the inertial range processes vary from purely nonlinear interacting components to less organized fluctuations (Velli et al. 1989; Bruno & Carbone 2013). The transition from $\zeta_2 \sim 2/3$ to $\zeta_2 \sim 1/2$ as r decreases gradually occurs and can be easily interpreted in the general framework of far-from-equilibrium complex systems as the evidence of a sort of dynamical phase transition which is consistent with the observed decreasing trend of positive correlation and the increasing of the outer scale with r (Chen et al. 2020). However, it is not sufficient to consider only one statistical moment of the probability distribution function to fully characterize solar wind turbulence. Indeed, since the pioneering work by Kolmogorov (1941) we know that turbulence is a phenomenon characterized by a hierarchy of scales whose statistics are scale-invariant (e.g., Kolmogorov 1941; Iroshnikov 1965; Kraichnan 1965; Frisch 1995; Alberti et al. 2019a). The statistical scale-invariance implies that the scaling of field increments should occur with a unique scaling exponent, thus implying that the statistical moments of the field increments should scale as $S_q(\tau) \sim \tau^{q/d}$, being $d = 3$ for fluid turbulence (e.g., Kolmogorov 1941; Frisch 1995) and $d = 4$ for plasma turbulence (e.g., Iroshnikov 1965; Kraichnan 1965; Bruno & Carbone 2013). Nevertheless, there is considerable evidence that turbulent flows deviate from this behavior, being the scaling exponents a nonlinear function of the order q (e.g., Carbone et al. 1995), which point out an "anomalous" scaling process and proves the appearence of intermittency (e.g., Frisch 1995; Bruno & Carbone 2013). For low orders the discrepancy with the linear behavior is very small, thus explaining why the Kolmogorov spectrum is usually observed in turbulence (e.g., $S_2(\tau) \sim \tau^{2/3} \rightarrow \mathcal{S}_2(f) \sim f^{-5/3}$). However, for high order statistics a difference is observed, and the breakdown of the statistical self-similarity is clear, thus questioning, in the modern theory of turbulence, what is really universal in the inertial range (e.g., Alberti et al. 2019b). Thus, for a proper characterization we investigate the behavior of scaling exponents ζ_q, $q \in [0, 5]$, as derived from the generalized Hilbert PSDs $\mathcal{S}_q(f)$ (cfr. Section 3), at different heliocentric distances as shown in Figure 4.

Firstly, a clear difference emerges from the scaling behavior for $r < 0.4$ au and for $r > 0.4$ au: the former is linear with q, while the latter shows the typical convex nonlinear shape with q. The surprisingly behavior of scaling exponents near the Sun, suggesting a monofractal nature of field fluctuations within the inertial range, supports the assumptions of global statistical self-similar scale-invariance. Conversely, these assumptions break at 0.4 au, where the nonlinear convex behavior of scaling exponents, suggest a multifractal behavior of magnetic field fluctuations (e.g., Bruno & Carbone 2013; Alberti et al. 2019a). This transition could be related to physical processes suppressing the scaling properties of the energy transfer rate close to the Sun, being consistent with the emergence of intermittency in solar wind turbulence for $r > 0.4$ au, also offering a novel scenario for the radial evolution of solar wind fractal nature for which, according to our knowledge, no exploration has been reported before in literature where only spectral features of field fluctuations were investigated at different locations (e.g., Bavassano et al. 1982; Denskat & Neubauer 1982; Grappin et al. 1990; Marsch & Tu 1990; Tu & Marsch 1990; Bruno & Carbone 2013; Marsch 2018; Chen et al. 2020). The results suggest that, since the intrinsic nature of magnetic field fluctuations within the inertial range moves from monofractal to multifractal, then there should be a bifurcation parameter describing the observed changes into the scaling properties, opening a new perspective in the framework of dynamical systems (e.g., Alberti et al. 2019b). The bifurcation parameter could be related to some plasma features as for example the β parameter, the magnetic compressibility, the expansion/correlation time of fluctuations within the inertial range, the slow-/Alfvénic-mode variability within the heliosphere, the outward propagating Alfvénic fluctuations (predominantly originating from the Sun but undergoing a dynamical evolution due to nonlinear and velocity-shear), localized phenomena giving rise to intermittency, local changes in the cross-helicity, and so on (Denskat & Neubauer 1982; Bavassano et al. 1982; Matthaeus & Goldstein 1982; Tu & Marsch 1990; Marsch & Tu 1990; Grappin et al. 1990; Carbone et al. 1995; Marsch 2018; Chen et al. 2020). Thus, the scaling exponents are not only a function of the statistical order q but they also depend on the radial distance r (i.e., $\zeta_q(r)$) which is the reflection of both global evolving and local dynamical processes. As also previously reported for spectral exponents, related to our findings by means of ζ_2, at different heliocentric distances (e.g., Denskat & Neubauer 1982; Marsch & Tu 1990; Tu & Marsch 1990; Chen et al. 2020), there seems to be a change as the Sun is approached, rather suddenly inside 0.4 au (Denskat & Neubauer 1982; Chen et al.

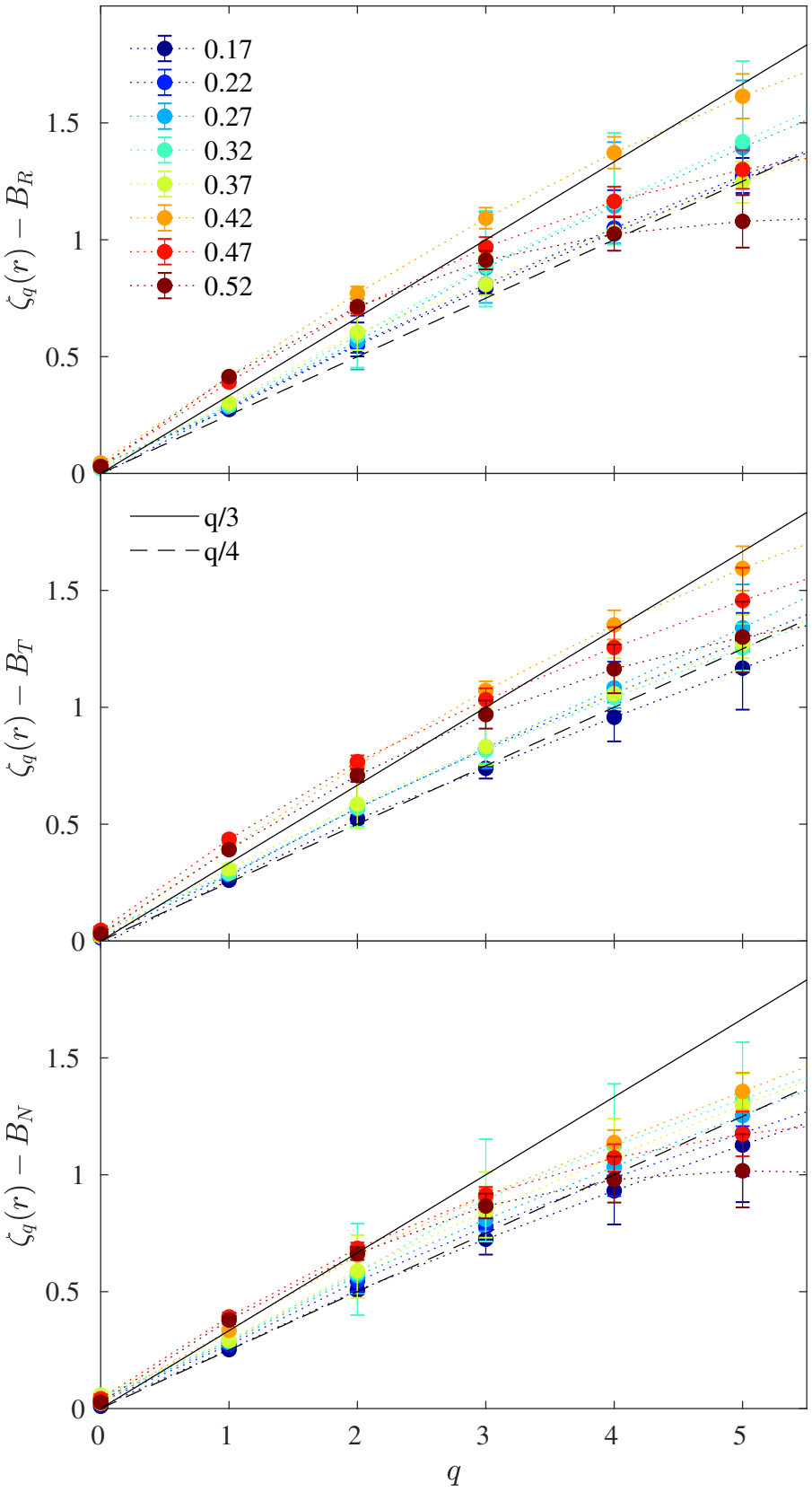

Figure 4. The behavior of the scaling exponents ζ_q for each magnetic field component at different heliocentric distances r. The different colors correspond to different distances r as reported in the legend. The continuous and dashed black lines are used as a reference to $q/3$ (Kolmogorov 1941) and $q/4$ (Iroshnikov 1965; Kraichnan 1965) theoretical scalings, respectively. Error bars show the 95% confidence level.

2020). Our findings not only strongly agree with seminal works when $q = 2$ is considered (e.g., Denskat & Neubauer 1982; Marsch & Tu 1990; Tu & Marsch 1990; Chen et al. 2020) but also allow, for the first time, to monitor the evolution of the scaling properties at different locations for high-order statistics, showing that the solar wind nature moves from monofractal to multifractal near 0.4 au. This change can be directly observed by looking at the behavior of singularities on the topology of solar wind magnetic field by means of the singularity strengths $\alpha(r) = \frac{d\zeta_q^\mu(r)}{dq}$ as usual in the multifractal approach (Frisch 1995; Bruno & Carbone 2013; Alberti et al. 2019a). In this way we can also provide a sort of multifractal measure $\Delta\alpha(r) = \max\{\alpha(r)\} - \min\{\alpha(r)\}$ (although we can only access the left part of the usual singularity spectrum $f(\alpha)$ since $q \geq 0$), thus allowing us to investigate the role of intermittency in changing the topology of the magnetic field. Fig. 5 reports the behavior of the multifractal width $\Delta\alpha(r)$ for each magnetic field component at different heliocentric distances r as in Fig. 4, while the inset show the behavior of singularity strengths $\alpha(r)$ at different distances r.

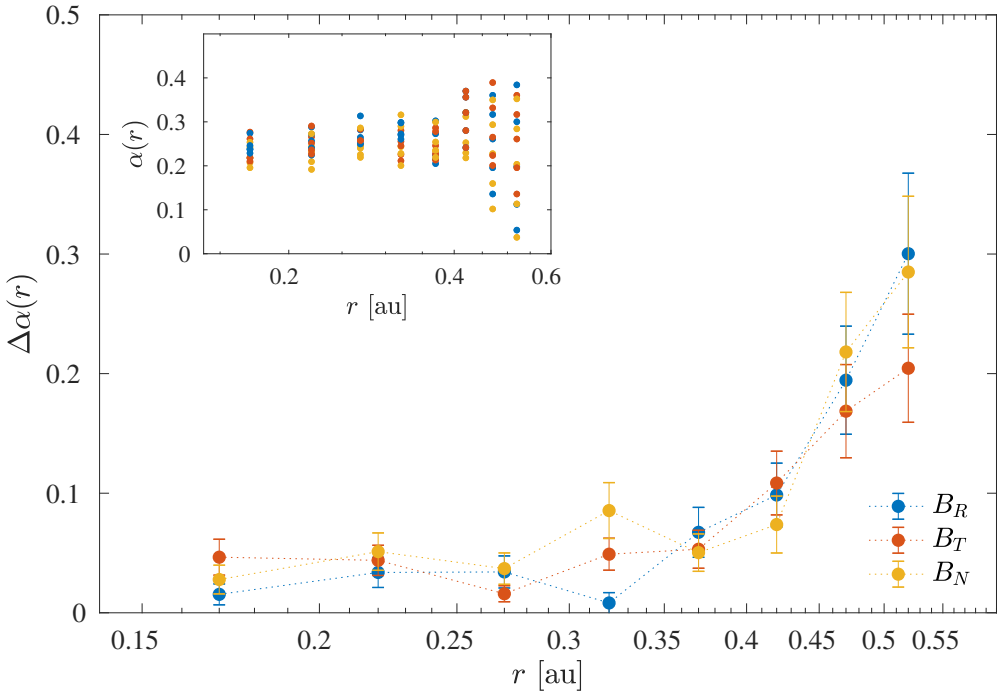

Figure 5. The behavior of the multifractal width $\Delta\alpha(r)$ for each magnetic field component at different heliocentric distances r as in Fig. 4. The blue, orange, and yellow symbols refer to the radial B_R, tangential B_T, and normal B_N components, respectively. Error bars show the 95% confidence level. The inset shows the behavior of $\alpha(r)$ at different distances r.

We clearly observe a breakdown of the multifractal width $\Delta\alpha(r)$, moving from values closer to zero up to larger values $\Delta\alpha(r > 0.4) > 0.2$, thus suggesting the emergence of singularities as r increases. This is confirmed by looking at the inset of Fig. 5 in which is easy to detect a spread in singularity strengths $\alpha(r)$ as r increases, with the transition observed near $r \sim 0.4$ au.

5. CONCLUSIONS

In this manuscript we dealt with the characterization of scaling features of magnetic field components as measured by PSP at different locations. We showed that the inertial range dynamics moves from a monofractal behaviour and a power spectrum scaling $f^{-3/2}$, at $r < 0.4$ au, to a multifractal one and a power spectrum scaling $f^{-5/3}$, at $r > 0.4$ au. This means that there is a transition region in which intermittency emerges, and the scaling properties of the inertial range are changed. Moreover, this also suggests that the solar wind magnetic field, in the early stages of its leaving the solar corona, show statistical self-similarity, while a breakdown of the statistical self-similarity for high-order statistics is found at a distance larger than 0.4 au from the Sun. In fact, we observed a roughly abrupt transition of the multifractal width $\Delta\alpha(r)$, moving from values closer to zero up to larger values $\Delta\alpha(r > 0.4) > 0.2$,

thus suggesting that wider singularities are found at $r > 0.4$, also confirmed by the spread in singularity strengths $\alpha(r)$ as r increases, with a transition observed near $r \sim 0.4$ au. Our results suggest that a dynamical phase transition occurs around 0.4 au and allow, for the first time, to characterize high-order statistics and the role of the intermittency in solar wind turbulence, suggesting that scaling exponents are not only a function of the statistical order q but they also depend on the radial distance r from the Sun, e.g., $\zeta_q(r)$, moving from a linear to a nonlinear convex behavior as r increases.

The observed transition could be related to something that suppresses the scaling properties of the energy transfer rate through the inertial range and the phase-coherency across the cascade for fluctuations close to the Sun. Roughly speaking, when the magnetic field is strong enough, since the scaling of the power spectra for inwards/outwards fluctuations are the same (Chen et al. 2020), the usual Iroshnikov-Kraichnan model suggests that fluctuations should scales as $\langle(\Delta b)^q\rangle \sim c_A\langle\epsilon_\ell^{q/4}\rangle\ell^{q/4}$, instead of the usual Kolmogorov scaling $\langle(\Delta b)^q\rangle \sim \langle\epsilon_\ell^{q/3}\rangle\ell^{q/3}$ (Bruno & Carbone 2013). In both cases, anomalous scaling laws $\zeta_q = hq + \mu(hq)$, being h either $h = 1/3$ or $h = 1/4$, are recovered through the fluctuations of the energy transfer rate being $\langle\epsilon_\ell^q\rangle \sim \ell^{\mu(q)}$. The combined effect of the strong Alfvénicity and the reduced compressibility observed close to the Sun (Chen et al. 2020) should for example suppress the scaling behavior of the energy transfer rate, thus making $\langle\epsilon_\ell^{q/4}\rangle \sim const.$ for $r < 0.4$ au, while leaving $\langle\epsilon_\ell^{q/3}\rangle \sim \ell^{\mu(q/3)}$ far from the Sun, thus providing an explanation for our observations.

These considerations can be described in a general framework of far-from-equilibrium complex systems as the evidence of a dynamical phase transition for the fractal nature of solar wind magnetic field fluctuations at different heliocentric distances r. Indeed, the observed change from a monofractal to a multifractal nature suggest that there exists perhaps a bifurcation parameter which needs to be related to plasma or wind parameters as the β parameter, the magnetic compressibility, the expansion/correlation time of fluctuations within the inertial range, the slow-/Alfvénic-mode variability, the outward/inward propagating Alfvénic fluctuations, the localized emergence of velocity-shear and/or local changes in the cross-helicity, and so on (Denskat & Neubauer 1982; Bavassano et al. 1982; Matthaeus & Goldstein 1982; Tu & Marsch 1990; Marsch & Tu 1990; Grappin et al. 1990; Carbone et al. 1995; Marsch 2018; Chen et al. 2020). In a simple conceptual model, being defined $\zeta_q^\mu(r)$ the scaling exponents of the magnetic field component $B_\mu(r)$ measured at the heliocentric distance r, can be written as

$$\zeta_q^\mu(r) = \sigma_\mu(r)\,(q + f(q, r))\,, \tag{14}$$

being $\sigma_\mu(r)$ the bifurcation parameter and $f(q, r)$ a smooth nonlinear convex function of q (e.g. Meneveau & Sreenivasan 1987; Carbone 1993; Bruno & Carbone 2013), slightly changing with r as a sort of sigmoid function. This also simply traduces into a general radial evolution of singularity strengths as

$$\alpha^\mu(r) = \alpha_0(r) + g(r, q), \tag{15}$$

thus interpreting the inset of Fig. 5 as a sort of bifurcation diagram resembling that derived in the case of saddle-node bifurcation, which can be also used for multifractal modeling purposes.

We are aware that by simply parametrizing solar wind conditions in terms of the heliocentric distance does not allow to directly discern on the typical solar wind parameters which could cause the observed bifurcation into the fractal nature of the inertial range. However, this is the simplest choice to deal with a complex system as the solar wind and its radial evolution, as also previously done by several authors (e.g., Denskat & Neubauer 1982; Tu & Marsch 1990; Chen et al. 2020). This means that the bifurcation parameter $\sigma_\mu(r)$ should depend, perhaps in a complex way, on the magnetic field intensity, the Alfvénicity of fluctuations, the presence of compressibility by slow-modes, the different ratio between plasma and magnetic pressures (i.e., the plasma β parameter), and so on (Chen et al. 2020). Future orbits of PSP at smaller r with hopefully a better temporal coverage of plasma parameters could allow to distinguish between the various possibilities.

We think that the observational evidence of a transition from a multifractal to a monofractal nature of solar wind magnetic field fluctuations across the inertial range as the Sun is approached and the novelty introduced by the Hilbert-Huang Transform method for overcoming some limitations (as stationarity and/or linearity) of classical methods (as structure function analysis and/or wavelet-based methods) offer new perspectives for describing the fractal properties of solar wind and to correctly characterize turbulence and intermittency in space plasma at different locations. Indeed, to our knowledge the observed bifurcation into the fractal nature has not been reported in literature before, being previous analysis on similar topics (e.g., Denskat & Neubauer 1982; Chen et al. 2020) mostly dealing on investigating

only the second-order statistical moment. Thus, in our opinion the results can be particularly useful for building up novel multifractal cascade models, mostly starting from seminal works (e.g., Meneveau & Sreenivasan 1987; Carbone 1993), for providing and testing new phenomenological models of the MHD turbulence (e.g., Lithwick et al. 2007), for considering the role of intermittency in modifying scaling features and scale-dependent behaviors (e.g., Mallet & Schekochihin 2017), as well as to characterize the role of the large-scale forcing and decaying mechanisms on the inertial range cascade (e.g., Chen et al. 2020). Further investigation will be devoted on the characterization the dynamical bifurcation occurring near $r = r_c \sim 0.4$ au in terms of a simple dynamical system admitting a saddle-node bifurcation as one or more control parameters are varied, although also different kind of bifurcations could be investigated (e.g., the super-critical pitchfork bifurcation) as well as its modeling in terms of (stochastic) Langevin systems or low-order discrete dynamical systems (Alberti et al. 2019b).

ACKNOWLEDGMENTS

The data used in this study are available at the NASA Space Physics Data Facility (SPDF), https://spdf.gsfc.nasa.gov/index.html. The FIELDS experiment on the Parker Solar Probe spacecraft was designed and developed under NASA contract NNN06AA01C. We acknowledge the contributions of the FIELDS team to the Parker Solar Probe mission. ML, GC, MFM, and VC thank the financial support by Italian MIUR-PRIN grant 2017APKP7T on Circumterrestrial Environment: Impact of Sun-Earth Interaction. The authors thank the anonymous reviewer for helpful comments improving our manuscript.

REFERENCES

Alberti, T., Consolini, G., De Michelis, P., Laurenza, M., & Marcucci, M. F. 2018, J. Space Weather Space Climate, 8, A56.

Alberti, T., Consolini, G., Carbone, V., Yordanova, E., Marcucci, M. F., & De Michelis, P. 2019, Entropy, 21, 320, doi:10.3390/e21030320.

Alberti, T., Consolini, G., & Carbone, V. 2019, Chaos, 29, 103107.

Alberti, T., Consolini, G., & Carbone, V. 2020, J. Phys. Conf. Ser., 1548, 012037.

Alberti, T., Lekscha, J., Consolini, G., De Michelis, P., & Donner, R. V. 2020, J. Space Weather Space Clim., 10, 25.

Bale, S. D., et al. 2016, Space Sci. Rev., 204, 49.

Bale, S. D., et al. 2019, Nature, 576, 237.

Belcher, J. W. 1971, ApJ, 168, 509.

Bavassano, B., Dobrowolny, M., Fanfoni, G., Mariani, F., & Ness, N. F. 1982, Sol. Phys., 78, 373.

Boldyrev, S. 2006, PhRvL, 96, 115002.

Bruno, R., & Carbone, V. 2013, Living Rev. Sol. Phys., 10, 2, https://doi.org/10.12942/lrsp-2013-2.

Burlaga, L. F., Klein, L., Sheeley, N. R. Jr., Michels, D. J., Howard, R. A., Koomen, M. J., Schwenn, R., & Rosenbauer, H. 1982, Geophys. Res. Lett., 9, 1317.

Carbone, V. 1993, PhRvL, 71, 1546.

Carbone, V. 1994, Ann. Geophys., 12, 585.

Carbone, V., Veltri, P., & Bruno, R. 1995, PhRvL, 75, 3110.

Carbone, F., Sorriso-Valvo, L., Alberti, T., et al. 2018, ApJ, 859, 27.

Carbone, F., Telloni, D., Bruno, A. G., et al. 2019, Atmosphere, 10, 611.

Chandran, B. D. G., Schekochihin, A. A., & Mallet, A. 2015, ApJ, 807, 39.

Chen, C. H. K. 2016, J. Plasma Phys., 82, 535820602.

Chen, C. H. K., et al. 2020, ApJS, 246, 53.

Consolini, G., Alberti, T., Yordanova, E., Marcucci, M. F., & Echim, M. 2017, J. Phys. Conf. Ser., 900, 012003.

Denskat, K. U., & Neubauer, F. M. 1982, J. Geophys. Res., 87, 2215.

Dobrowolny, M., Mangeney, A., & Veltri, P. 1980, PhRvL, 45, 144.

Dudok de Wit, T. 2004, PhRvE, 70, 055302.

Fox, N. J., Velli, M. C., Bale, S. D., et al. 2016, Space Sci. Rev., 204, 7, doi:10.1007/s11214-015-0211-6.

Frisch, U. 1995 Turbulence. The Legacy of A. N. Kolmogorov, Cambridge University Press, Cambridge, UK, ISBN 0-521-45713-0.

Grappin, R., Mangeney, A., & Marsch, E. 1990, J. Geophys. Res.,95 , 8197.

Horbury, T. S., Forman, M., & Oughton, S. 2008, PhRvL, 101, 175005.

Howard, R. A., et al. 2019, Nature, 576, 232.

Howes, G. G., Bale, S. D., Klein, K. G., et al. 2012, ApJL, 753, L19.

Huang, N. E., Shen, Z., Long, S. R., et al. 1998, P. Roy. Soc. Lond. A, 454, 903.

Huang, Y. X., Schmitt, F. G., Lu, Z. M., et al. 2008, EPL (Europhysics Letters), 84, 40010.

Huang, Y., Schmitt, F. G., Lu, Z., et al. 2009, Journal of Hydrology, 373, 103.

Huang, Y. X., Schmitt, F. G., Hermand, J.-P., et al. 2011, PhRvE, 84, 016208.

Iroshnikov, P. S. 1965, Sov. Astron., 7, 556.

Kasper, J. C., et al. 2019, Nature 576, 228.

Klein, K. G., Howes, G. G., TenBarge, J. M., et al. 2012, ApJ, 755, 159.

Kolmogorov, A. N. 1941, Dokl. Akad. Nauk SSSR, 30, 301.

Kraichnan, R. H. 1965, Phys. Fluids, 8, 1385.

Laurenza, M., Alberti, T., Marcucci, M. F., et al. 2019, ApJ, 873, 112.

Lithwick, Y., Goldreich, P., & Sridhar, S. 2007, ApJ, 655, 269.

Mallet, A., & Schekochihin, A. A. 2017, MNRAS, 466, 3918.

Marsch, E., & Tu, C.-Y. 1990, J. Geophys. Res., 95, 8211, doi:10.1029/JA095iA06p08211.

Marsch, E. 2018, Ann. Geophys., 36, 1607.

Marsden, R., & Fleck, B. 2003, Adv. Space Res., 32, 2699.

Matthaeus, W. H., & Goldstein, M. L. 1982, J. Geophys. Res., 87, 6011.

McComas, D. J., Barraclough, B. L., Gosling, J. T., Hammond, C. M., Phillips, J. L., Neugebauer, M., Balogh, A., & Forsyth, R. J. 1995, J. Geophys. Res., 100, 19893.

McComas, D. J., et al. 2019, Nature, 576, 223.

Meneveau, C., & Sreenivasan, K. R. V. 1987, PhRvL, 59, 1424.

Milillo, A., Fujimoto, M., Kallio, E., et al. 2010, Planetary and Space Science, 58, 40.

Müller, D., Marsden, R. G., St. Cyr, O. C., et al. 2013, Sol. Phys., 285. 25.

Nicolaou, G., Verscharen, D., Wicks, R. T., & Owen, C. J. 2019, ApJ, 886, 101.

Parker, E. 1958, ApJ, 128, 664.

Perez, J. C., & Boldyrev, S. 2009, PhRvL, 102, 025003

Politano, H., Pouquet, A., & Carbone, V. 1998, Europhys. Lett., 43 516.

Rosenbauer, H., Schwenn, R., Marsch, E., Meyer, B., Miggenrieder,H., Montgomery, M. D., Mühlhäuser, K.-H.,Pilipp, W., Voges,W., & Zink, S. M. 1977, J. Geophys. Res., 42, 561.

Tu, C.-Y., & Marsch, E. 1990, J. Geophys. Res., 95, 4337.

Velli, M., Grappin, R., & Mangeney, A. 1989, PhRvL, 63, 1807.

Verscharen, D., Chen, C. H. K., & Wicks, R. T. 2017, ApJ, 840, 106.

Zhao, L.-L., Zank, G.P., Adhikari, L., Nakanotani, M., Telloni, D., & Carbone, F. 2020, ApJ, 898, 113.